Astron. Astrophys. 341, 163–173 (1999)

ASTRONOMY AND ASTROPHYSICS

A search for star formation in the translucent clouds MBM7 and MBM55⋆

T. Hearty[1], **L. Magnani**[2], **J.-P. Caillault**[2], **R. Neuhäuser**[1], **J.H.M.M. Schmitt**[3], **and J. Stauffer**[4]

[1] Max-Planck-Institut für Extraterrestrische Physik, D-85740 Garching, Germany (e-mail: thearty@xray.mpe.mpg.de)
[2] Department of Physics and Astronomy, University of Georgia, Athens, GA 30602, USA
[3] Hamburger Sternwarte Universität Hamburg, Gojenbergsweg 112, D-21029 Hamburg, Germany
[4] Harvard/Smithsonian Center for Astrophysics, Cambridge, MA 02138, USA

Received 12 May 1998 / Accepted 24 September 1998

Abstract. The star formation capability of two molecular clouds at high galactic latitude ($|b| > 30°$) is investigated. Possible pre-main sequence stars in and around the translucent clouds MBM7 and MBM55 have been identified via their X-ray emission by inspecting *ROSAT* All-Sky Survey observations of the clouds and environs and *ROSAT* pointed observations of the high-density cores within the clouds. Follow-up optical spectroscopy of the stellar X-ray sources with $V \leq 15.5$ mag was conducted with the 1.5-m Fred Lawrence Whipple Observatory telescope to identify standard signatures of pre-main sequence stars (LiI λ6708 Å absorption and Hα emission). We found 11 stars which have lithium equivalent widths, W(Li), above our detection threshold. Three of the stars with lithium also have weak Hα emission. Relative ages for the stars with lithium are estimated by their position on an W(Li) vs. $T_{\rm eff}$ diagram. A calibration derived from data for several clusters with known ages indicates the stars are older than the translucent high-latitude clouds. This conclusion is supported by a comparison with theoretical evolutionary tracks of the stars from our sample for which we have distance measurements from Hipparcos. We find it is unlikely that any of the X-ray active, lithium-rich stars we identified have formed in the clouds in question. Theoretical and observational arguments support this conclusion and render unlikely the possibility that low-extinction translucent clouds are the sites of star formation.

Key words: ISM: clouds – stars: formation

1. Introduction

In the last decade over 100 small molecular clouds have been found at $|b| \geq 30°$ and are known collectively as "high-latitude molecular clouds" (Blitz et al. 1984; Magnani et al. 1985 [hereafter, MBM]; Keto & Myers 1986; Heiles et al. 1988). An up-to-date compilation of these objects, most of which fall into the category of translucent clouds, is presented by Magnani et al. (1996b). Translucent clouds are usually defined as molecular clouds with visual extinction in the range $1 \leq A_v \leq 5$ mag (van Dishoeck & Black 1988). Because translucent clouds have intermediate properties between diffuse clouds and dark clouds, the question of whether the translucent clouds form stars is open. Answering this question is important since understanding the physical conditions in the lowest density gas which can give rise to stars may elucidate the mechanism(s) responsible for low-mass star formation.

In the first few years after the identification of high-latitude molecular clouds, these objects were regarded as essentially low-density versions of dark clouds (similar to those in Taurus) with average volume densities ≤ 500 cm^{-3} and a dearth of any high-density regions. In ensuing years, small, dense regions in some translucent clouds were identified (Mebold et al. 1987; Turner et al. 1989; Turner et al. 1992; Turner 1993a,b,c). Reach et al. (1995) estimated the densities of the cores in several translucent clouds from maps of the rotational emission lines of CS to be at least $10^{4.5}$ cm^{-3} in regions which have typical diameters ~ 0.06 pc. Since the density rises steeply with decreasing radius in dense cores (e.g., $n \propto r^{-2}$ in CS-emitting regions and possibly steeper depending on the molecular tracer [Reach et al. 1995]), the cores appear superficially similar to those found in dark clouds and giant molecular clouds where the association between dense molecular cores and young stars is well established (see, Lada (1993) for a review). Thus, star formation may be possible in translucent molecular clouds.

Moreover, in recent years there have been a growing number of pre-main sequence (PMS) stars identified at high galactic latitude with T Tauri-like characteristics. We have updated the list presented by Magnani et al. (1995) of currently known (or suspected) T Tauri stars (TTS) at high galactic latitude and provided available Hα and LiI λ6708 Å equivalent widths in Table 1. Although there have been several surveys for TTS at high galactic latitudes, none of the TTS in Table 1 have been associated with *translucent* molecular clouds. The most extensive of these surveys have searched for TTS with strong Hα emission (Kun 1992; Martín & Kun 1995) and infrared excess (Magnani et al. 1995; Palla et al. 1997). However, these properties

Send offprint requests to: T. Hearty

⋆ Table 3 is only available in electronic form at the CDS via anonymous ftp to cdsarc.u-strasbg.fr (130.79.128.5) or via http://cdsweb.u-strasbg.fr/Abstract.html.

Table 1. T Tauri stars at $|b| \geq 30^\circ$

Cloud	Star	RA [2000]	Dec [2000]	l [deg]	b [deg]	SpT	V [mag]	W(Hα) [Å]	W(LiI) [Å]	Ref.
···	CP-53 295	1:17:47	−52:33:10	293.7	−64.1	F2	10.5	−5.0	···	1,2
···	Hen 1	2:10:07	−55:29:53	281.7	−58.3	K	9.9	−0.2	0.09	3,4
···	02538+1953	2:56:39	+20:05:42	158.9	−33.9	···	12.7	···	···	2,5
···	RXJ0324.4+0231	3:24:25	+02:31:01	180.2	−42.7	K5	12.4	−0.4	0.33	6,7,8
···	RXJ0333.2+1035	3:33:12	+10:35:56	174.6	−35.6	K3	11.7	−0.8	0.32	
···	RXJ0344.9+0359	3:33:53	+03:59:31	183.1	−37.9	K3	12.4	0.3	0.30	
···	RXJ0354.4+0535	3:54:21	+05:35:41	183.4	−35.0	G1	10.3	3.5	0.20	
MBM12	LkHα262	2:56:08	20:03:24	158.8	−34.0	M0	14.6	−34.4	···	9,10
(L1453,4)	LkHα263	2:56:08	20:03:38	158.8	−34.0	M2	14.6	−19.6	···	
(L1457,8)	LkHα264	2:56:38	20:05:37	158.9	−33.9	K5	12.5	−89.6	···	2,9,10,11
	02553+2018	2:58:12	20:30:07	159.0	−33.3	K3	10:	−5.0	···	2,12
MBM13	S18	3:02:20	17:10:35	162.3	−35.5	M	>13.5	em	···	13
MBM18	$\sim$ 6 stars									14
(L1569)										
MBM20	L1642-1a,b	4:35:02	−14:13:41	210.9	−36.6	K7	13.5	em	···	2,15,16
(L1642)	L1642-2a,b	4:34:50	−14:13:08	210.8	−36.6	···	···	···	···	2,15
···	04451-0539a	4:47:34	−5:34:14	203.2	−30.0	···	14.8	−20.0	0.71	4,5
···	04451-0539b	4:47:34	−5:34:14	203.2	−30.0	···	15.3	−42.0	···	4,5
···	HD98800Aa	11:22:04	−24:46:30	278.4	33.8	K5V	9.6	>0.1	0.43	2,4,17,18
···	HD98800Ba					K7V	10.0	···	0.34	18
···	HD98800Bb					M1V	···	···	0.45	18
···	RXJ1410.8-2355	14:10:50	−23:55:28	325.3	35.5	K2	11.7	···	0.51	19
···	RXJ1412.2-1630	14:12:14	−16:29:53	329.5	42.2	G9	11.4	···	0.31	19
···	RXJ1419.3-2322	14:19:21	−23:22:13	327.8	35.2	K0	9.6	···	0.34	19
MBM33	K35a	15:34:55	−7:21:49	357.8	37.5	M4V	···	−4.2	0.61	20
	K35b	15:34:55	−7:21:49	357.8	37.5	M5IV	15.3	−8.5	0.69	20
	K37	15:35:08	−6:55:33	358.3	37.8	M4.5IV	···	−8.3	0.61	20
MBM37	K54	15:50:43	−3:58:53	4.3	36.7	M5.5IV	···	−14.9	0.81	20
···	S202	23:22:24	−2:13:50	78.6	−57.2	mid-F	12.6	−19.0	···	1,2,5,21,22

(1) Gregorio-Hetem et al. (1992) identify this object as an Herbig Ae/Be star. (2) Magnani et al. (1995). (3) Henize (1976) identifies this object as an emission-line K star. (4) Gregorio-Hetem et al. (1992) identify this object as a T Tauri star. (5) Whitelock et al. (1995); identified as a T Tauri Star. (6) Neuhäuser et al. (1995b); Possibly associated with Taurus. (7) Magazzù et al. (1997). (8) Neuhäuser et al. (1997). (9) Herbig & Bell (1988). (10) Fernández et al. (1995). (11) Gameiro et al. (1993). (12) Caillault et al. (1995). (13) Downes & Keyes (1988); object could be an Me star. (14) Brand et al. (in preparation); the candidates all show excess Hα emission but they have not yet been conclusively identified with T Tauri stars. (15) Sandell et al. (1987); both L1642-1 and -2 are visual binaries. (16) Liljeström et al. (1989). (17) Worley & Douglass (1997). (18) Soderblom et al. (1996). (19) Wichmann et al. (1997); possible Gould Belt members near Lupus. (20) Martín & Kun (1995); K35A,B is a binary. (21) Downes & Keyes (1988); identified as a T Tauri star. (22) Zuckerman (private communication); probably a post-main sequence star.

are most commonly associated with "classical" TTS (CTTS). Since "weak" TTS (WTTS), which are most often identified by their strong X-ray emission, are not typically associated with a large infrared excess and they lack strong Hα emission (e.g., Walter et al. 1988), they would not necessarily stand out from the normal field star population in these surveys. Although Caillault et al. (1995) searched the *Einstein* X-ray satellite images which overlap with high-latitude molecular clouds for TTS possibly associated with these clouds, only 6 of the clouds in their survey are translucent clouds and the *Einstein* overlap with these clouds is only ~ 2.1 deg^2. Therefore, the search for WTTS in translucent clouds is largely incomplete.

Although several of the recently discovered TTS listed in Table 1 have been associated with dark clouds, most do not seem to be associated with any molecular material (see Table 1 and references therein). For example, one of the seemingly isolated TTS, HD98800, may be associated with the TW Hya association, a possible association of TTS not projected against any star forming molecular cloud (e.g., Kastner et al. 1997). Fekel & Bopp (1993) argued that this system is ≤ 10 Myr based on the measurement of lithium in the components and estimated the distance to be ~ 34 pc (i.e., more distant than a main sequence star of similar apparent magnitude). The measured parallax from the Hipparcos satellite places this star at a distance of 47 ± 6 pc which supports the young age proposed by Fekel & Bopp.

If the TTS described above are not associated with any known molecular cloud, where did they originate? If the stars are very young ($\sim$ a few $\times 10^6$ years), there are two possibilities for their origin: (1) they formed in clouds that have since dissipated (Feigelson 1996) or (2) they were ejected by dynamical

interactions within distant star forming regions with velocities of several km s^{-1} (e.g., Sterzik & Durisen 1995). An alternative interpretation is that some of these stars are misidentified as young isolated objects but are in fact older objects ($\sim 10^8$ yr) that have escaped from older star formation regions with a thermal drift velocity $v \sim 1$–2 km s^{-1} (Feigelson 1996). More recently, Guillout et al. (1998) suggest that RASS detected stars projected on or near the Gould belt (a nearby population of stars that may tie together most of the nearby star forming regions) are the low mass counterparts to the higher mass stars that first defined the Gould Belt and these stars actually form a disk rather than a belt. If the Gould Belt is really a disk rather than a belt it may explain the origin of these young stars found at high galactic latitude away from the Gould Belt. Although there is still much debate about the precise age of these stars, because they have not yet depleted their lithium they are considered to be young stars with ages $\leq 10^8$ years.

X-ray observations of star forming regions have revealed a large population of previously undetected PMS stars (e.g., Walter et al. 1988, Neuhäuser 1997). Thus, we used the *ROSAT* Position Sensitive Proportional Counter (PSPC) to locate X-ray active stars in the direction of three translucent clouds at high galactic latitude that represent differing types of translucent molecular clouds (both kinematically and chemically). The primary method was to investigate *ROSAT* All-Sky Survey (RASS) data in large regions in and around MBM7, MBM40, and MBM55 to identify any X-ray stars in the vicinity of these clouds because the true extent of the molecular gas is not well known and TTS can sometimes be displaced several parsecs from their parent clouds (e.g., Neuhäuser et al. 1995b). The secondary method was to study deep *ROSAT* pointed observations of the cores in these translucent clouds. Finding young stars spatially coincident with the molecular cores would present the most compelling evidence that star formation is ongoing in these low-mass clouds. The results of the X-ray search for star formation in the isolated, compact, gravitationally bound molecular cloud MBM40 have already been published (Magnani et al. 1996a). We now present the results of a similar search in MBM7 and MBM55.

2. The sample

The two translucent molecular clouds investigated in this paper are emblematic of the low visual extinction ($A_v < 3$ mag) clouds that are the most common type of cloud identified at high galactic latitude (MBM). However, both of these clouds contain dense cores similar to the cores found in star forming dark clouds and the possibility of star formation is greater than in an object like MBM40 which does not have dense cores (Magnani et al. 1996a). Not surprisingly, the previous search for star formation in the isolated gravitationally bound cloud MBM40 found no star formation taking place there (Magnani et al. 1996a). A comparison of this cloud with other high-latitude star forming clouds where gravity plays differing roles (e.g., MBM12, not gravitationally bound; MBM20, gravitationally bound) has revealed that gravitational binding of the entire cloud is neither a necessary nor sufficient condition for star formation to take place.

In this paper we investigate whether compression by shocks is a sufficient trigger for star formation in high-latitude clouds. MBM7 and MBM55 are situated within two large arcs of dust and gas as seen in infrared and radio observations (Verter et al. 1998; Gir et al. 1994). These arcs have most likely been swept-up by a supernova or possibly stellar winds. The shocks which accompany the sweeping up of interstellar gas are ideal triggers for the star formation process (e.g., Elmegreen 1993). The filamentary morphology of these clouds, perhaps indicative of their genesis in a swept-up HI shell, makes them excellent examples of clouds in which this type of mechanism may have triggered star formation.

2.1. MBM7

MBM7 is a large (≥ 1.2 deg^2) high-latitude cloud located at (l,b) $\sim (150\overset{\circ}{.}4, -38\overset{\circ}{.}1)$ southwest of the Taurus-Auriga complex of dark molecular clouds. Although Lynds (1965) identified several bright nebulae in this region it is not listed in the Lynds (1962) catalog of dark clouds. It was first identified as a molecular entity by MBM and its distance was established from star counts by Magnani & de Vries (1986) to be 125 ± 50 pc. The central region of MBM7 differs markedly from most high latitude clouds in that the CO(J=1-0) antenna temperature is quite high (5-6 K) and is more typical of dark rather than translucent clouds. However, Magnani & de Vries (1986) estimate the visual extinction in the central region of MBM7 at ~ 2 magnitudes. Thus, MBM7 is most likely a translucent cloud with a centrally condensed region of size ~ 1 pc.

Minh et al. (1996) have recently mapped the central 0.75 deg^2 of the cloud in HI, ^{12}CO(J=1-0), and ^{13}CO(J=1-0) and found evidence for a centrally condensed region with a mass ~ 5 M$_\odot$ in which there are at least 3 high density ($n \geq 2000$ cm^{-3}) cores that do not seem to be gravitationally bound. However, a smaller, central clump in MBM7 with size ~ 0.036 pc, shows very strong CS(J=2-1) emission (Reach et al. 1995). A multi-wavelength, large-velocity gradient (LVG) analysis (cf., Goldreich & Kwan 1974) of the three lowest rotational levels of CS in a sample of high-latitude clouds by Reach et al. (1995) found that the central clump of MBM7 has a dense ($n \sim 10^5$ cm^{-3}) molecular core which may be gravitationally bound. If the core has sufficient time to collapse before the cloud dissipates, then it is a possible site for the formation of stars in the 0.1 - 0.5 M$_\odot$ range. The controversy between the bound/unbound nature of the clumps in MBM7 may be due to the different gas tracers used in the two analyses. Regardless of the gravitational state of the smallest clumps in the cloud, MBM7 represents a compact cloud which is gravitationally unbound at least on the larger scales, and is embedded in an HI arc associated with several other high-latitude molecular clouds (Fig. 1).

At this stage it is unclear if this infrared arc is mostly molecular and thus similar to the MBM53-55 complex (see Sect. 2.2), or whether the arc is mostly atomic with a few molecular condensations embedded throughout. Whether the hydrogen in this

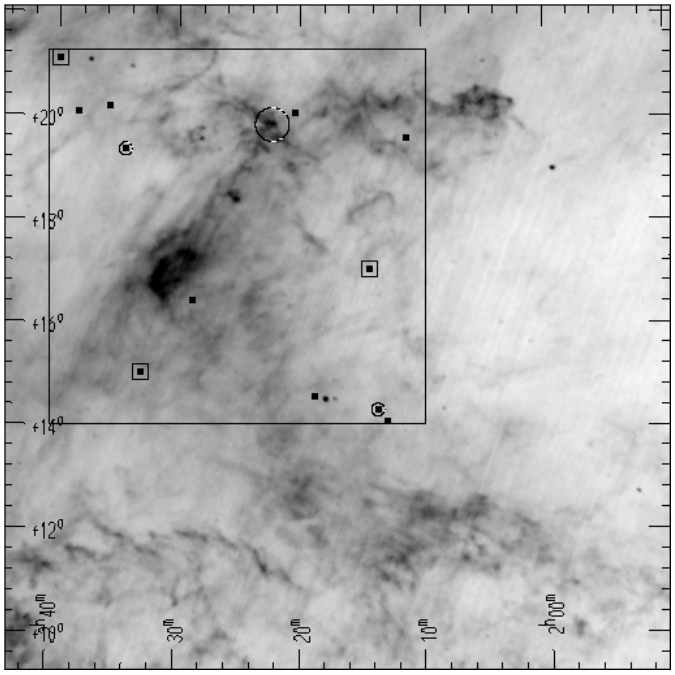

Fig. 1. The stellar X-ray sources detected in the RASS observation of the MBM7 complex are marked with squares on an IRAS 100 μm image of the HI arc associated with MBM5-9 and G154.7-39.8. A box is drawn around the region in which we investigated the RASS data and the large circle located at (α,δ) $\sim$ ($2^{\rm h}22^{\rm m}$,20°) in the northern portion of the arc shows the inner 20′ field of view of the *ROSAT* pointed observation of MBM7. The stars which show Hα emission are circled and those that show LiI absorption are marked with concentric open squares. The bright feature at (α,δ) $\sim$ ($2^{\rm h}30^{\rm m}$,17°) is the molecular cloud G154.7-39.8. The coordinates of this and all subsequent images are J2000.

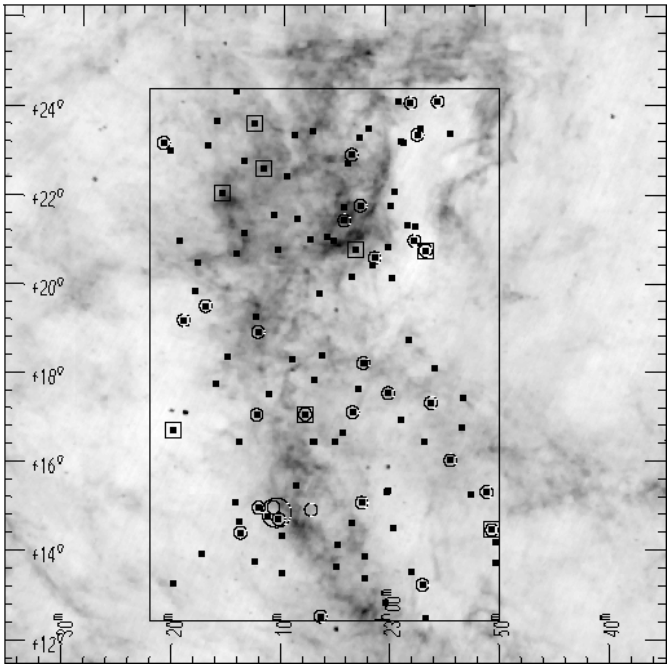

Fig. 2. The stellar X-ray sources detected in the RASS observation covering MBM53-55 are marked with squares on an IRAS 100μm image showing the high-latitude cloud complex. A box is drawn around the region in which we investigated the RASS data and the large circle marks the inner 20′ field of view of the *ROSAT* pointed observation of MBM55. The stars which show Hα emission are circled and those that show LiI absorption are marked with concentric open squares. The two small circles without corresponding small squares mark the positions of Hα emission stars detected in the *ROSAT* pointed observation of this cloud but not in the RASS. One of these stars is located outside of the inner 20′ field of view of the *ROSAT* PSPC but we mark its position because it was identified as a dMe star by Martín & Kun (1995).

complex is mostly molecular or atomic, G154.7-39.8 is the most prominent infrared component of the arc. Although the significant infrared emission of G154.7-39.8 is most likely associated with a large column density of gas, the molecular component of this particular cloud has not been mapped.

2.2. MBM55

MBM55 located at (l,b) $\sim$ (89.°2,$-$40.°9) is similar to MBM7 in that it is embedded in a region containing a large filamentary HI structure within which there are several other molecular clouds (Fig. 2). However, MBM55 is the largest translucent cloud identified by MBM and has the greatest spatial extent ($>$ 4 deg^2) and mass ($>$ 300 M$_\odot$) of any molecular cloud at $|b| \geq 30.°$ The HI arc includes several other MBM clouds (53, 54, and possibly 56) associated with MBM55 and extends at least from $b = -30°$ to $-40.°$ We will refer to the entire region as the MBM55 complex. The distance estimates to all three of these molecular clouds have a large degree of uncertainty (Welty et al. 1989); MBM53, 110 pc $\leq d \leq$ 155 pc; MBM54, 145 pc $\leq d \leq$ 260 pc; MBM55, 30 pc $\leq d \leq$ 156 pc. However, assuming the three clouds are physically associated, a good estimate for the distance to the cloud complex is $\sim$ 150 pc. The molecular clouds are embedded in a large HI arc that appears to be expanding at 10-13 km s^{-1} (Gir et al. 1994) and covers more than 30 deg^2 of the high-latitude sky. The only other molecular structure this large at $|b| \geq 25°$ is the Polaris Flare (Heithausen & Thaddeus 1990). However, unlike the Polaris Flare, the MBM55 cloud complex is clearly separated from the galactic plane and is the best example of a high-latitude molecular cloud complex associated with, and probably formed in, a swept-up HI shell (e.g., Elmegreen 1988).

The morphology of MBM55 shown by the (incomplete) map in MBM consists of a filamentary structure with a series of clumps embedded in a lower density substrate. A few of the clumps show extended CS(J=2-1) emission that implies H$_2$ densities as high as a few $\times$ 10^4 cm^{-3} (Reach et al. 1995; Vallee & Koempe 1993). In fact, the region around the largest clump, (α,δ) $\sim$ ($23^{\rm h}08^{\rm m}$,+15°06′), has enough dust associated with it so that the reflection from the dust on the red POSS plate was misidentified as an extended HII region by Sharpless (1959). Therefore MBM55 also shows evidence for high density regions that may be possible sites for star formation.

3. X-ray observations

We investigated the RASS data in a 53 deg^2 area around MBM7 and a 91 deg^2 area around MBM55 and identified all of the X-ray sources with a maximum likelihood for existence, ML > 8, and at least 8 counts above the local background in at least one of the energy bands described below. The maximum likelihood can be converted into probability P through the equation P = 1 $-$ exp($-$ML). In addition we identified all of the X-ray sources above a similar threshold in the inner 20′ radius of two *ROSAT* PSPC pointed observations (one of each cloud). The *ROSAT* exposure times and limiting broad band fluxes and luminosities at the assumed cloud distances are listed in Table 2. Details about *ROSAT* and its PSPC detector can be found in Trümper (1983) and Briel & Pfeffermann (1995), respectively. The X-ray source search was conducted in different *ROSAT* standard "bands", defined as follows: "soft" = 0.1–0.4 keV; "hard" = 0.5–2.0 keV; "hard1" = 0.5–0.9 keV; "hard2" = 0.9–2.0 keV; "broad" = 0.1–2.0 keV. The hard band X-ray images of the regions studied are displayed in Fig. 3.

3.1. X-ray data reduction

The data were reduced in a manner similar to that described in detail by Neuhäuser et al. (1995a). The X-ray sources were identified using the LDETECT, MDETECT, and MAXLIK algorithms of the Extended Scientific Analysis Software System (EXSAS) of the MPE (Zimmermann et al. 1993) which runs under the European Southern Observatory Munich Image Data Analysis System (ESO-MIDAS). The LDETECT algorithm identifies sources using a "sliding window" technique which utilizes a local background surrounding the detection cell while the MDETECT algorithm uses a full field-of-view map of the expected instrumental background in conjunction with the photon and particle background estimates. The source lists derived from LDETECT and MDETECT are then subjected to a maximum likelihood analysis (MAXLIK) which fits the observed distribution of counts to a background model across the region of interest and a point source. The best fit is the most likely value for the background and source counts, and source position. More detailed descriptions of these algorithms can be found in Cruddace et al. (1988) and Zimmermann et al. (1993).

3.2. Results of the X-ray observations

We identified a total of 309 X-ray sources above our detection threshold. Twenty-five sources are from the RASS observation of MBM7, 217 from the RASS observation of MBM55 and 47 and 20 from the *ROSAT* pointed observations of each cloud. All of the X-ray sources were cross-referenced with the SIMBAD[1] and NED[2] databases to remove non-PMS stars and extra-galactic objects; 16 cataloged extragalactic objects were removed from the RASS observation of MBM55 via this procedure. In addition we inspected the Guide Star Catalog and the Digitized Sky Survey images in 40″ circles around each X-ray source to identify possible optical counterparts to the X-ray sources (Neuhäuser et al. 1995a). In this fashion, two previously uncatalogued galaxies were identified by inspection of the Digitized Sky Survey images. Also, estimates of the optical magnitude allowed us to calculate the X-ray to optical flux ratio (log[f$_x$/f$_v$]):

$$\log(f_x/f_v) = \log Z_{\rm B} + 0.4V - 5.08$$

where $Z_{\rm B}$ is the *ROSAT* broad-band count rate and V is the visual magnitude of the optical counterpart (Sterzik & Durisen 1995). Given the errors in the measured X-ray flux and the estimated visual magnitudes, the error in the estimate of log(f_x/f_v) is ~ 0.3.

Results of the *Einstein* Extended Medium Sensitivity Survey (EEMSS) show that among extragalactic sources all but a few have log(f_x/f_v) > -1.0; in addition, those few exceptions are normal galaxies which are easy to identify on the POSS plates. All stars (except 7 dMe stars with $0.0 >$ log(f_x/f_v) > -1.0) including the TTS detected in the EEMSS, have log(f_x/f_v) < -1.0 (Stocke et al. 1991). Although previous *Einstein* results did not identify any stars with a log(f_x/f_v) > 0.0, the larger database of the *ROSAT* telescope has identified some white dwarfs that have log(f_x/f_v) > 0.0 (Motch et al. 1997). Fleming et al. (1996) estimate there to be about 175 white dwarfs detected in the RASS. Therefore if we assume they are uniformly distributed in the sky, we predict there to be ~ 0.004 white dwarfs deg^{-2} and thus we do not expect there to be more than the one white dwarf detected in the regions we investigated. Since one cataloged white dwarf was detected in the RASS observation of MBM7 most (if not all) of the remaining sources with log(f_x/f_v) > 0.0 are extragalactic. Since we are looking for X-ray active, PMS stars and, in many cases, making rough estimates of the visual magnitude as seen on the Digitized Sky Survey images, we adopt a conservative cut-off for selecting possible PMS stars. All sources which have log(f_x/f_v) > 0.0 are considered to be extragalactic and those with log(f_x/f_v) < 0.0 are considered to be stellar objects, some of which could be PMS. Using the X-ray to optical flux ratio criteria, 136 sources (12 from the RASS observation of MBM7 and 31 from the pointed observation and 87 from the RASS observation of MBM55 and 6 from the pointed observation) were eliminated from our list of objects for further study since their

Table 2. *ROSAT* observations of the high-latitude clouds investigated

Cloud	SEQID	Exposure [ks]	$f_{\rm x,lim} \times 10^{15}$ [erg cm^{-2} s^{-1}]	log$L_{\rm x,lim}$ [erg s^{-1}]
MBM7	RASS	0.2	420	29.9
	900147	25.4	11	28.3
MBM55	RASS	0.4	220	29.8
	900173	8.5	20	28.7

[1] This research has made use of the SIMBAD database, operated at CDS, Strasbourg, France.

[2] The NASA/IPAC Extragalactic Database (NED) is operated by the Jet Propulsion Laboratory, Caltech, under contract with the National Aeronautics and Space Administration.

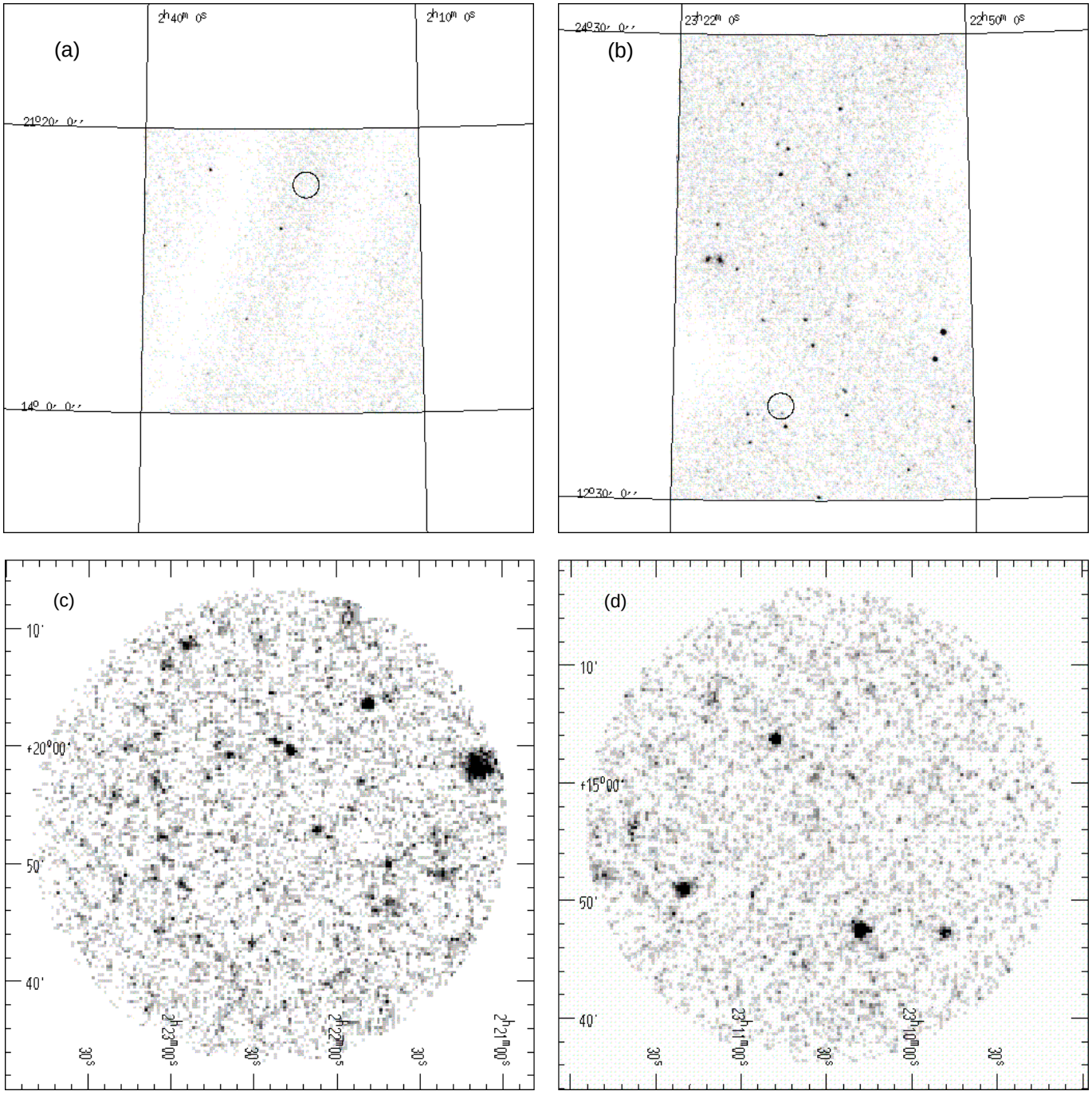

Fig. 3a–d. The RASS "hard band" (0.5–2.0 keV) images of the regions investigated around MBM7 and MBM55 are displayed in **a** and **b**, respectively. The circles represent the inner 20′ fields of view of the *ROSAT* pointed observations of each cloud displayed in **c** and **d**. Only a few sources were detected in the RASS observations of MBM7 because of the short exposure time (~ 200 s) of the RASS in this region of the sky.

high X-ray to optical flux ratio ($\log[f_x/f_v] > 0.0$) precludes them from being stars (Stocke et al. 1991).

We list the *ROSAT* names and source positions of the remaining 155 X-ray sources in Table 3, along with the maximum likelihood for existence for each source, the broad band count rates, the X-ray hardness ratios $HR1$ and $HR2$ (as defined by Neuhäuser et al. 1995a), the apparent visual magnitude, and the broad band X-ray to optical flux ratio. We also list the spectral type and the Hα and lithium equivalent widths of the sources that have been observed spectroscopically. In addition, we include one star (RXJ2307.3+1501) that was found to have Hα in emission by Martín & Kun (1995) but was detected 47′ off axis in the *ROSAT* PSPC pointed observation of MBM55. Since many of the stellar candidates in Table 3 have X-ray hardness ratios similar to TTS (e.g., Neuhäuser et al. 1995a) they were considered as possible young stars associated with MBM7 and

MBM55 and were thus candidates for follow-up optical spectroscopy to search for other indicators of youth.

4. Optical observations

Typically, each X-ray source had only one or two possible stellar optical counterparts within its 40″ error circle, hence there were a total of 179 possible optical counterparts which required follow-up optical spectroscopy. We observed spectroscopically all optical counterparts down to a visual magnitude threshold of $V \sim 15.5$ mag for the sources detected in the RASS-I data set[3]. However, the X-ray data presented here are the RASS-II results which detected several sources that were not found in the RASS-I data set and therefore were not observed spectroscopically. The follow-up observations for the RASS-II set are thus $\sim$ 80% complete to a limiting visual magnitude of $\sim$ 15.5 mag. Since all but 13 of the un-observed objects have $-1 < \log(f_x/f_v) < 0$, they are probably mostly either M stars or extragalactic objects (e.g., Stocke et al. 1991).

The optical spectra were obtained from September 29 through October 2 of 1995 using the FAST spectrograph with the 600 lines mm^{-1} grating of the 1.5-m Fred Lawrence Whipple Observatory telescope. The 1.″5 slit size provided a reciprocal dispersion of $\sim$ 0.75 Å pixel^{-1}. The wavelength range of the spectra ($\sim$ 5500-7500 Å) was selected to detect two indicators of possible youth (Hα emission & LiI λ6708 Å absorption) and to determine spectral types. As a rule, the smallest measurable equivalent width in units of mÅ is approximately the reciprocal dispersion in units Å mm^{-1} (Jaschek & Jaschek 1987). Therefore, given the 15μm pixels of the CCD used for the observations, the smallest measurable equivalent width for these spectra is $\sim$ 50 mÅ (0.05 Å). Since this is less than the typical equivalent width of most TTS we expect the follow-up spectral observations to identify the LiI λ6708 Å feature if there are any TTS in our sample of X-ray selected objects. All spectra were given an initial inspection at the telescope. If a particular star showed signs of youth or the integration produced fewer than $\sim$ 1000 cts pixel^{-1}, at least one additional integration was performed. Fig. 4 displays the 6500 to 6750 Å region of our spectra which show LiI absorption.

The 12 F, G, and K stars in which lithium has been detected are listed in Table 4. The effective temperatures given in the table are taken from the calibration of de Jager & Nieuwenhuijzen (1987) based on their spectral type and assuming they are luminosity class V stars (unless some other luminosity class is given). Three of the K stars in the direction of MBM55 that show LiI absorption also have weak Hα emission. In addition to the stars with lithium, we also observed 17 dMe stars and 13 dKe stars that show weak (i.e., W[Hα] > -10Å)[4] Hα emission but no lithium absorption. The uncertainty in W(Li) is $\sim$ 0.06 Å as determined by the mean standard deviation of multiple measurements of the LiI λ6708 Å doublet in known TTS using the same optics.

[3] The first processing of the RASS is known as the RASS-I data while the second processing is known as the RASS-II data. Details on the differences can be found in Voges et al. (1996). The main difference is that the RASS-II reduction merged the data into 1378 overlapping sky-fields rather than $2^\circ \times 360^\circ$ strips. The RASS-II processing resulted in better determined count rates because of the improved background map and fewer spurious sources because of an improved aspect solution.

Table 4. Effective temperatures of stars with LiI detections

Star	SpT	log($T_{\rm eff}$)[a] [K]	W(Hα) [Å]	W(Li) [Å]
RXJ0214.3+1704	K0	3.712 ± 0.014	1.95	0.20
RXJ0232.8+1502[b]	F8V	3.796 ± 0.010	3.23	0.14
RXJ0239.9+2106	G3	3.757 ± 0.012	2.94	0.26
RXJ2250.4+1431	K1	3.698 ± 0.014	-0.27	0.08
RXJ2253.0+1650[b,c]	K1III	3.654 ± 0.013	0.55	0.04
RXJ2256.3+2052a	K7	3.618 ± 0.012	-1.07	0.15
RXJ2303.1+2055[b]	G5V	3.745 ± 0.007	3.78	0.08
RXJ2307.9+1710a	K7	3.618 ± 0.012	-1.85	0.10
RXJ2312.0+2245	G3	3.757 ± 0.012	3.00	0.09
RXJ2313.0+2345	F8	3.796 ± 0.010	3.46	0.25
RXJ2316.1+2210	G5	3.745 ± 0.007	2.43	0.10
RXJ2320.4+1647	K2	3.685 ± 0.014	1.08	0.18

[a] The log($T_{\rm eff}$) are taken from de Jager & Nieuwenhuijzen (1987) assuming the stars are luminosity class V objects (unless another luminosity class is indicated). The errors given assume an uncertainty in spectral type of $\sim$ 1 subtype. However, if the uncertainty in luminosity class is taken into account, the errors could be a factor of 3 larger.
[b] This star was observed with Hipparcos (see Sect. 5.2).
[c] The Hα and lithium equivalent widths of this star were taken from high resolution measurements by Fekel & Balachandran (1993).

5. Inferred ages

5.1. The stars with lithium

Since lithium abundance is a model dependent quantity that can be inferred if one knows the lithium equivalent width, $T_{\rm eff}$, and surface gravity of a particular star, we have chosen an observational technique that searches for all stars that could *possibly* be TTS based on the observational criteria that they are bright X-ray sources and have lithium equivalent widths similar to known TTS. However, if one of the assumed parameters (i.e., temperature or gravity) are different than for typical TTS, the large lithium equivalent widths could be the result of these phenomena rather than its presumed youth. Also, older post-main sequence giant stars can sometimes show strong lithium absorption lines in their spectra (e.g., de la Reza et al. 1997). However, these objects are rare and not typically X-ray bright, therefore most stars that satisfy our selection criteria probably are young.

Although the LiI absorption and X-ray activity (and Hα emission for three of the K stars) indicate that these stars are probably young objects, these properties are often still present in stars with ages $\sim 10^8$ yr (e.g., Briceño et al. 1997). If these stars formed in MBM7 or MBM55, they should have ages similar to the lifetimes of the clouds (a few $\times 10^6$ yr), otherwise

[4] The negative sign denotes emission.

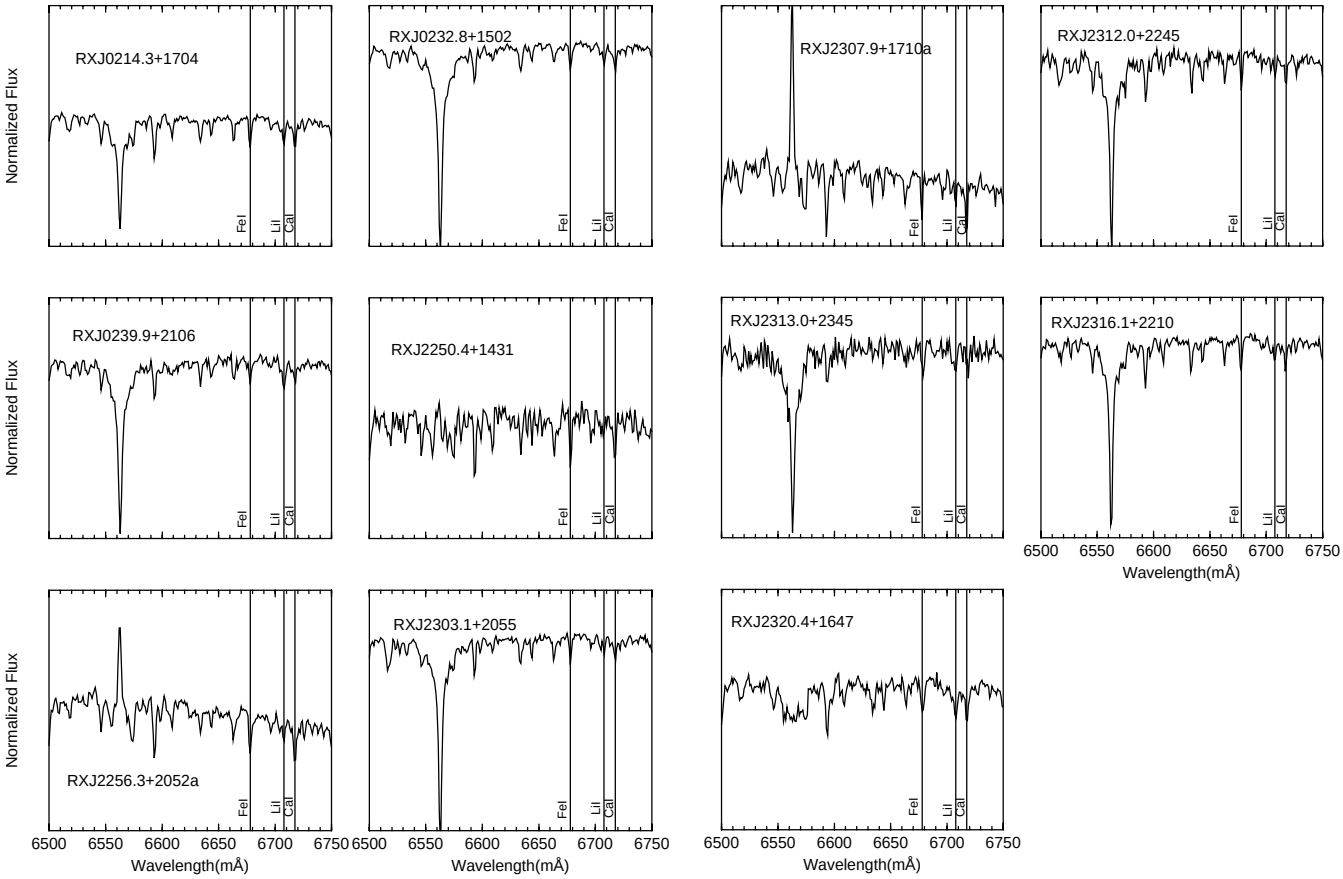

Fig. 4. Spectra of the 11 X-ray stars in which lithium has probably been detected. The Hα line ranges from absorption to weak emission. The weak lithium features in two of these stars (RXJ2250.4+1431 & RXJ2303.1+2055) should be confirmed with higher resolution spectra.

they may be part of the foreground population of young stars with ages $\sim 10^8$ yr predicted by Briceño et al. (1997). Since we do not have measured parallaxes for most of these stars, we cannot place them all on the HR diagram to estimate their ages from a comparison with theoretical isochrones (however, see Sect. 5.2). However, we can plot the stars on an W(Li) vs. $T_{\rm eff}$ diagram and determine less accurate relative ages by comparing them with different age groups of stars (e.g., Briceño et al. 1997; Magazzù et al. 1997; Neuhäuser et al. 1997). In Fig. 5 we compare our stars with stars in Taurus, the Pleiades, the Hyades and the TTS from Table 1. The location of most of the TTS from Table 1 in the figure suggests they have ages similar to or slightly older than the TTS in Taurus ($\sim$ a few $\times\, 10^6$ yr). However, the measured W(Li) for most of the stars in the direction of MBM7 and MBM55 in which we detected lithium is consistent with their being roughly the age of the Pleiades ($\sim 10^8$ yr) or the Hyades ($\sim 8 \times 10^8$ yr)[5]. Although there is little distinction in W(Li) between T Tauri and Pleiades age stars hotter than around 5000 K (log$T_{\rm eff}$ $\sim$ 3.7) because the shallow convection zones of these stars do not allow for efficient PMS lithium depleting, two stars (one in the direction of MBM7 [RXJ0239.9+2106] and one in the direction of MBM55 [RXJ2313.0+2345]) with $T_{\rm eff}$ $\sim$ 6000 K have a larger W(Li) than similar spectral type stars in the Pleiades and therefore may be young enough to be associated with these clouds.

However, the surface densities of the X-ray bright stars with lithium detected in the RASS observations of MBM7, MBM40, and MBM55 are $\sim$ 0.06 stars deg^{-2}, 0.0 stars deg^{-2}, and $\sim$ 0.1 stars deg^{-2}, respectively. Since these surface densities are equivalent to (or less than) the observed surface density of high-latitude lithium-rich yellow stars detected in the EEMSS ($\sim$ 0.1 stars deg^{-2}; Sciortino et al. 1995), it is likely that the X-ray detected stars with lithium in the direction of MBM7 and MBM55 are part of the same population detected in the *Einstein* observations. Since $\sim$ 98% of the *Einstein* observations at high galactic latitude were not pointed at high latitude clouds, our observations strongly indicate that there is no enhancement of lithium-rich X-ray active stars in the direction of high-latitude clouds.

5.2. Theoretical evolutionary tracks and X-ray luminosities of the stars observed with Hipparcos

Seventeen of the X-ray identified stars in the direction of MBM7 and MBM55 were also observed with the Hipparcos satellite and therefore have measured parallaxes that allow us to cal-

[5] However, Neuhäuser & Brandner (1998) found a few stars with lithium as low as the Pleiades which are pre-main sequence according to their Hipparcos data.

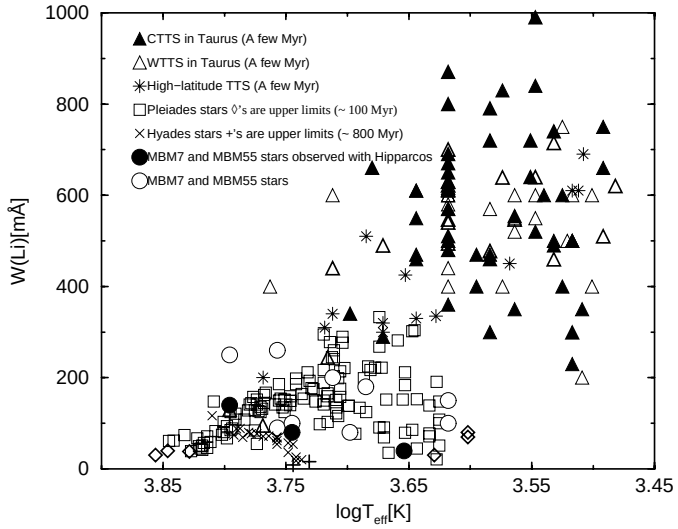

Fig. 5. W(Li) vs. log$T_{\rm eff}$ diagram. The 12 stars from Table 4 are compared with several populations of stars with known age. The CTTS in this diagram have W(Hα) < -10 Å and the WTTS have W(Hα) > -10 Å. The data for the stars in Taurus are from Strom et al. (1989); Basri et al. (1991); Patterer et al. (1993); Marcy et al. (1994); Martín et al. (1994). The Pleiades and Hyades data are from Soderblom et al. (1993) and Soderblom et al. (1990), respectively.

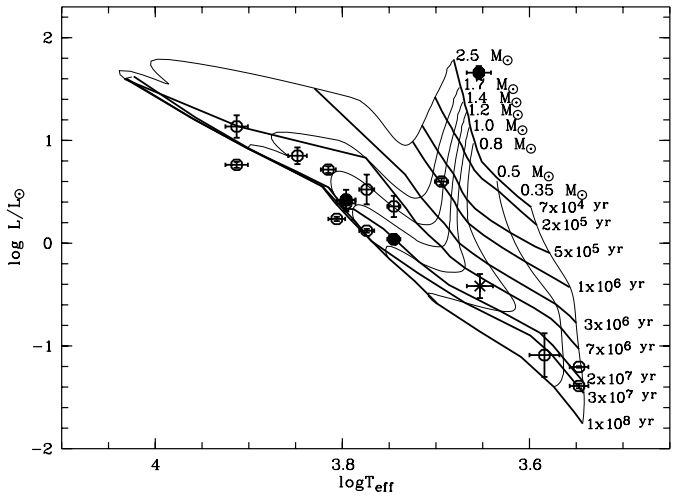

Fig. 6. The X-ray detected stars from our sample that were observed with Hipparcos are plotted in an HR diagram with theoretical PMS evolutionary tracks of D'Antona & Mazzitelli (1998) with Alexander opacities, and the convection formulation of Canuto & Mazzitelli (1992), X = 0.02, Y = 0.28, and a deuterium mass fraction 2×10^{-5}. The filled circles represent the stars in which lithium has been detected and open circles represent those with no published measurement of the lithium equivalent width. In addition we plot HD98800 (asterisk) the only T Tauri star at high galactic latitude known to be observed with Hipparcos. The two stars (RXJ2253.0+1650 and RXJ2305.1+1633) well above the main sequence are post-main sequence stars that have lithium equivalent widths below our detection threshold.

culate X-ray and bolometric luminosities and place the stars on the HR diagram. The results of the Hipparcos observations and the derived parameters are listed in Table 5. Effective temperatures and bolometric corrections were taken from de Jager & Nieuwenhuijzen (1987) and Zombeck (1990), respectively, based on spectral type. The broad band X-ray luminosities were calculated based on the X-ray count rates and $HR1$ values listed in Table 3 using the X-ray count rate to flux conversion factor given by Schmitt et al. (1995).

The distances calculated from the Hipparcos parallaxes for these stars show that both of the stars in the direction of MBM7 (RXJ0232.9+1502 & RXJ0235.8+2012) are foreground objects that happen to be located along the line of sight to the cloud. However, the uncertainty in the distance of MBM55 is large enough that most of the stars in that direction could be relatively near the cloud. Only three of the stars in the direction of MBM55 (RXJ2256.6+1633, RXJ2303.1+2055, & RXJ2306.5+1954) can be identified as foreground objects based on Hipparcos distances. Three of the stars observed with Hipparcos (RXJ0232.9+1502, RXJ2303.1+2055, & RXJ2253.0+1650) are also listed in Table 4 since they were found to have weak lithium absorption. However, two of these (RXJ0232.9+1502 & RXJ2303.1+2055) are foreground objects and one (RXJ2253.0+1650) is a post-main sequence RS CVn binary (Fekel & Balachandran 1993).

We plot the stars from Table 5 on an HR diagram with theoretical PMS evolutionary tracks from D'Antona & Mazzitelli (1998) in Fig. 6. The three stars in which lithium has been detected are marked with filled circles and those with no detected lithium are marked with open circles. For comparison, we also plot HD98800 (asterisk) the only T Tauri star at high galactic latitude known to be observed with Hipparcos. The two stars (RXJ2253.0+1650 and RXJ2305.1+1633) located well above the main sequence in the figure are two post-main sequence luminosity class III and IV sources both of which have W(Li) measurements below our detection threshold[6]. All of the remaining sources are found to lie close to (or just slightly above) the main sequence in the diagram. However, a few stars are located between the 7 and 20 million year isochrones. Since the PMS star HD98800 is also between these isochrones this figure suggests that these stars are as young as HD98800. However, none of the stars in this region of the diagram were found to contain lithium, whereas HD98800 shows strong lithium absorption. Therefore the stars in the direction of MBM55 are probably older, unresolved binaries along the line of sight to the cloud.

The X-ray luminosities of all but the 5 most X-ray luminous stars in Table 5 are less than that of similar spectral type stars in the Pleiades (Stauffer et al. 1994), thus their X-ray luminosities are consistent with the ages for the stars in which lithium was detected (i.e., their ages are equivalent to or older than the Pleiades). In addition, except for the 1 post-main sequence RS CVn binary, RXJ2253.0+1650, the stars in Table 5 have X-ray luminosities less than or equal to the least X-ray luminous stars in the X-ray luminosity function for the WTTS

[6] Fekel & Balachandran (1993) detected lithium with an equivalent width below our detection threshold in a high resolution spectrum of the RS CVn binary RXJ2253.0+1650.

Table 5. X-ray detected stars observed with Hipparcos

Name	HIP	distance [pc]	V [mag]	SpT	log$T_{\rm eff}$ [K]	log$(L/L_\odot)$	logL_x [erg s^{-1}]
RXJ0232.9+1502[a]	11843	28.7 ± 0.7	6.0	F8V	3.796 ± 0.010	0.42 ± 0.02	29.4 ± 0.1
RXJ0235.8+2012	12097	14.0 ± 0.4	10.7	M2	3.547 ± 0.012	-1.39 ± 0.02	27.7 ± 0.4
RXJ2253.0+1650[a]	112997	96.8 ± 7.1	5.9	K1III	3.654 ± 0.013	1.66 ± 0.06	31.5 ± 0.1
RXJ2255.6+1811	113211	134.2 ± 16.9	7.7	A5	3.913 ± 0.012	1.14 ± 0.11	29.6 ± 0.4
RXJ2256.6+1633	113296	6.9 ± 0.1	8.7	M2:	3.547 ± 0.012	-1.20 ± 0.01	27.2 ± 0.2
RXJ2257.9+1336	113398	91.9 ± 8.6	7.5	F2	3.848 ± 0.010	0.85 ± 0.08	29.1 ± 0.4
RXJ2258.8+1703	113476	139.1 ± 23.2	9.2	G0	3.774 ± 0.008	0.52 ± 0.14	29.7 ± 0.4
RXJ2303.1+2055[a]	113829	24.3 ± 0.5	6.7	G5V	3.745 ± 0.007	0.04 ± 0.02	29.1 ± 0.1
RXJ2305.1+1633	113994	40.4 ± 1.5	6.4	G8IV	3.694 ± 0.007	0.60 ± 0.03	28.5 ± 0.3
RXJ2306.3+1830	114081	43.2 ± 1.6	6.2	F6Vs	3.815 ± 0.008	0.72 ± 0.03	29.2 ± 0.2
RXJ2306.4+1236	114088	36.6 ± 8.9	11.5	M0:	3.584 ± 0.016	-1.09 ± 0.21	29.5 ± 0.3
RXJ2306.5+1954	114096	28.3 ± 0.7	6.4	F7V	3.806 ± 0.009	0.24 ± 0.02	28.9 ± 0.1
RXJ2307.0+1758	114149	94.3 ± 11.1	8.6	F8	3.796 ± 0.010	0.42 ± 0.10	29.5 ± 0.4
RXJ2307.4+2108	114189	39.9 ± 1.4	6.0	A5V	3.913 ± 0.012	0.76 ± 0.03	28.3 ± 0.3
RXJ2309.1+1824	114320	95.7 ± 11.4	8.8	G5	3.745 ± 0.007	0.36 ± 0.10	29.5 ± 0.3
RXJ2310.0+1425	114378	25.9 ± 0.6	6.5	G0V	3.774 ± 0.008	0.12 ± 0.02	29.4 ± 0.1
RXJ2316.3+1750	114893	85.1 ± 7.9	8.4	F8	3.796 ± 0.010	0.39 ± 0.08	29.2 ± 0.4

[a] This star was found to have lithium.

in Taurus (e.g., Neuhäuser 1997). Therefore, the *ROSAT* and Hipparcos observations show the stars in Table 5 are not WTTS and thus did not form in MBM7 or MBM55.

6. Conclusions

Although we cannot place all the stars in our sample on an HR diagram to determine more accurate ages, based on the relative age calibration of the stars plotted in the W(Li) vs. $T_{\rm eff}$ diagram (Fig. 5), we conclude that, at best, MBM7 and MBM55 have each formed a ~ 1 M$_\odot$ star that might *possibly* be younger than the Pleiades (i.e., they have a larger lithium equivalent width than similar spectral type stars in the Pleiades). However, since neither of these stars are projected near the cores in MBM7 and MBM55, it is doubtful that they formed in these clouds. In addition, because this study of two clouds associated with HI shells found no clearcut evidence of recent star formation, it is likely that the sweeping up of diffuse gas *at high galactic latitudes* is not an effective agent for initiating star formation in the translucent clouds embedded in HI shells.

Although the stars we have detected are too old to be associated with translucent molecular clouds, some are young enough to have retained much of their lithium. Therefore these observations have added new members to the growing list of nearby X-ray active stars with ages ≤ 150 Myr, predicted by current age dependent stellar population models (e.g., Guillout et al. 1996). In addition, if the Gould Belt is really a disk rather than a belt as suggested by Guillout et al. (1998), some of these lithium-rich yellow stars found at higher galactic latitude may be Gould Belt members.

Since other methods making use of Hα and infrared observations to search for star formation at high galactic latitude also did not find TTS associated with translucent clouds (Martín & Kun 1995; Magnani et al. 1996b; Palla et al. 1997), our study coupled with the previous surveys indicates that the star formation rate of low-extinction translucent molecular clouds is substantially lower than for dark clouds or even higher extinction translucent molecular clouds at high galactic latitude. The total mass of MBM7, MBM40, and MBM55 is ≥ 400 M$_\odot$. If we assume masses ~ 1.2 M$_\odot$ for the one F8 in the direction of MBM55 and ~ 1.0 M$_\odot$ for the one G3 star in the direction of MBM7 that *may* be PMS stars associated with these clouds, we can calculate an absolute upper limit of $\sim 0.6\%$ for the star formation efficiency of these three translucent clouds.

Acknowledgements. We wish to thank Juan Alcalá for helpful discussions and assistance in preparing Fig. 6 and Ben Zuckerman for comments on Table 1. In addition, Patrick Guillout provided helpful comments concerning the relation of these stars to the large scale distribution of X-ray active stars detected with *ROSAT*. We thank an anonymous referee for many valuable suggestions. The *ROSAT* project is supported by the Max-Planck-Gesellschaft and Germany's federal government (BMBF/DLR). TH is grateful for grants from the Max-Planck-Gesellschaft and the UGA Graduate School Assistantship for support of this research. Partial support for this work was obtained from NASA grant NAG 5-2666 to LM and NASA grant NAG 5-1610 to JPC. RN acknowledges a grant from the Deutsche Forschungsgemeinschaft (DFG Schwerpunktprogramm "Physics of star formation").

References

Basri G., Martín E.L., Bertout C., 1991, A&A 252, 625
Blitz L., Magnani L., Mundy L., 1984, ApJ 282, 9
Briceño C., Hartmann L., Stauffer J., et al., 1997, AJ 113, 740
Briel U.G., Pfeffermann E., 1995, In: Siegmund O.H., Vallerga J.V. (eds.) Proc. SPIE Vol. 2518, EUV, X-ray, & Gamma-Ray Instrumentation for Astronomy VI. 120
Caillault J.-P., Magnani L.A., Fryer C., 1995, ApJ 441, 261

Canuto V.M., Mazzitelli I., 1992, ApJ 389, 724
Cruddace R.G., Hasinger G.R., Schmitt J.H.M.M., 1988, In: Murtagh F., Heck A. (eds.) ESO Conference and Workshop Proc. 28, Astronomy from Large Databases. Garching, 177
Cutispoto G., Tagliaferri G., Pallavicini R., Pasquini L., Rodonó M., 1996, A&AS 115, 41
D'Antona F., Mazzitelli I., 1998, In: Micela G., Pallavicini R. (eds.) Cool Stars in Clusters and Associations. In press
de Jager C., Nieuwenhuijzen H., 1987, ApJ 177, 217
de la Reza R., Drake N.A., da Silva L., Torres C.A.O., Martìn E.L., 1997, ApJ 482, L77
Downes. R.A., Keyes C.D., 1988, AJ 96, 777
Elmegreen B.G., 1988, ApJ 326, 616
Elmegreen B.G., 1993, In: Levy E., Luinine J. (eds.) Protostars and Planets III. University of Arizona Press, 97
Feigelson E., 1996, ApJ 468, 306
Fekel F., Balachandran S., 1993, ApJ 403, 708
Fekel F., Bopp B., 1993, ApJ 419, L89
Fernández M., Ortiz E., Eiroa C., Miranda L.F., 1995, A&A 114, 439
Fleming T.A., Snowden S.L., Pfeffermann E., Briel U., Greiner J., 1996, A&A 316, 147
Frasca A., Catalano S., 1994, A&A 284, 883
Gameiro J.F., Lagor M.T.V., Lima N.M., Cameron A.C., 1993, MNRAS 261, 11
Gir B.-Y., Blitz L., Magnani L., 1994, ApJ 434, 162
Goldreich P., Kwan J., 1974, ApJ 189, 441
Gregorio-Hetem J., Lépine J.R.D., Quast G.R., Torres C.A.O., de la Reza R., 1992, AJ 103, 549
Guillout P., Haywood M., Motch C., Robin A.C., 1996, A&A 316, 89
Guillout P., Sterzik M., Schmitt J.H.M.M., Motch C., Neuhäuser R., 1998, A&A, in press
Harju J., Walmsley C.M., Wouterloot J.G., 1993, A&AS 98, 51
Heiles C., Reach W.T., Koo B.-C., 1988, ApJ 332, 313
Heithausen A., Thaddeus P., 1990, ApJ 353, L49
Henize K.G., 1976, ApJS 30, 491
Herbig G.H., Bell K.R., 1988, Lick Observatory Bulletin No. 1111
Jaschek C., Jaschek M., 1987, The Classification of Stars. Cambridge University Press, Cambridge
Kastner J.H., Zuckerman B., Weintraub D.A., Forveille T., 1997, Sci 277, 67
Keto E.R., Myers P.C., 1986, ApJ 304, 466
Kun M., 1992, A&AS 92, 875
Lada C.J., 1993, In: Yuan C., You J. (eds.) Molecular Clouds and Star Formation. World Scientific, 1
Liljeström T., Mattila K., Friberg P., 1989, A&A 210, 337
Lynds B.T., 1962, ApJS 7, 1
Lynds B.T., 1965, ApJS 12, 163
Magazzù A., Martín E.L., Sterzik M.F., et al., 1997, A&AS 124, 449
Magnani L., Blitz L., Mundy L., 1985, ApJ 295, 402
Magnani L., Caillault J.-P., Buchalter A., Beichman C.A., 1995, ApJS 96, 159
Magnani L., Caillault J.-P., Hearty T., et al., 1996a, ApJ 465, 825
Magnani L., Hartmann D., Speck B., 1996b, ApJS 106, 447
Magnani L., de Vries C.P., 1986, A&A 168, 271
Marcy G.W., Basri G., Graham J.R., 1994, ApJ 428, L57
Martín E.L., Kun M., 1995, A&AS 116, 467
Martín E.L., Rebolo R., Magazzú A., Pavlenko Ya.V., 1994, A&A 282, 503
Mebold U., Heithausen A., Reif K., 1987, A&A 180, 213
Minh Y.C., Park Y.-S., Kim K.-T., et al., 1996, ApJ 467, 717
Motch C., Guillout P., Haberl F., et al., 1997, A&A 318, 111
Myers P.C., 1985, In: Black D.C., Matthews M.S. (eds.) Protostars and Planets II. U. of Arizona Press, Tucson, 81
Neuhäuser R., 1997, Sci 276, 1363
Neuhäuser R., Brandner W., 1998, A&A 330, 29
Neuhäuser R., Sterzik M.F., Schmitt J.H.M.M, Wichmann R., Krautter J., 1995a, A&A 297, 391
Neuhäuser R., Sterzik M.F., Torres G., Martín E.L., 1995b, A&A 299, L13
Neuhäuser R., Torres G., Sterzik M.F., Randich S., 1997, A&A 325, 647
Palla F., Codella R., Valdettaro R., Baffa C., 1997, A&A 327, 755
Patterer R.J., Ramsey L., Huenemoerder D.P., Welty A.D., 1993, AJ 105, 1519
Reach W., Pound M., Wilner D., Lee Y., 1995, ApJ 441, 244
Sandell G., Reipurth B., Gahm G., 1987, A&A 181, 283
Schmitt J., Fleming T., Giampapa M., 1995, ApJ 450, 392
Sciortino S., Favata F., Micela G., 1995, Sci 296, 370
Sharpless S., 1959, ApJS 4, 257
Soderblom D.R., Oey M.S., Johnson D.R.H., Stone R.P.S., 1990, AJ 99, 595
Soderblom D.R., Jones B.F., Balachandran S., et al., 1993, AJ 106, 1059
Soderblom D., Henry T., Shetrone M., Jones B., Saar S.H., 1996, ApJ 460, 984
Stauffer J.R., Caillault J.-P., Gagné M., Prosser C.F., Hartmann L.W., 1994, ApJS 91, 625
Sterzik M.F., Durisen R.H., 1995, A&A 304, L9
Stocke J.T., Morris S.L., Gioia I.M., et al., 1991, ApJS 76, 813
Strom K., Wilkin F., Strom S., Seaman R., 1989, AJ 98, 1444
Trümper J., 1983, Adv. Space Res. 2, 241
Turner B.E., 1993a, ApJ 405, 229
Turner B.E., 1993b, ApJ 410, 140
Turner B.E., 1993c, ApJ 411, 219
Turner B.E., Rickard L.-J, Xu L.-P., 1989, ApJ 344, 292
Turner B.E., Xu L., Rickard L.J., 1992, ApJ 391, 158
Vallee J.P., Koempe C., 1993, AJ 106, 1561
van Dishoeck E.F., Black J.H., 1988, ApJ 334, 771
Verter F., Magnani L., Dwek E., Rickard L.-J, 1998, ApJ, submitted
Voges W., Boller T., Dennerl K., et al., 1996, MPE Report 263, 637
Walter F.M., Brown A., Mathieu R.D., Myers P.C., Vrba F.J., 1988, AJ 96, 297
Welty D.E., Hobbs L.M., Blitz L., Penprase D.E., 1989, ApJ 346, 232
Whitelock P., Menzies J., Feast M., et al., 1995, MNRAS 276, 219
Wichmann R., Sterzik M., Krautter J., Metanomski A., Voges W., 1997, A&A 326, 211
Worley C.E., Douglass G.G., 1997, A&AS 125, 523
Zimmermann H.U., Belloni T., Izzo C., Kahabka P., Schwentker O., 1993, EXSAS Users' Guide, MPE report 244, ROSAT Scientific Data Center, Garching
Zombeck M.V., 1990, Handbook of Space Astronomy & Astrophysics. Cambridge University Press